DOI: 10.22226/2410-3535-2018-4-384-400 PACS: 61.48.Gh; 61.72.Bb; 61.72.Lk; 61.72.Mm

Disclinations in polycrystalline graphene and pseudo-graphenes. Review

A. E. Romanov[1,2,†], M. A. Rozhkov[1], A. L. Kolesnikova[1,3]

[†]alexey.romanov@niuitmo.ru

[1]ITMO University, 49 Kronverksky ave., St. Petersburg, 197101, Russia
[2]Ioffe Institute, 26 Polytechnicheskaya str., St. Petersburg, 194021, Russia
[3]Institute of Problems of Mechanical Engineering, 61 Bolshoj ave., Vas. Ostrov, St. Petersburg, 199178, Russia

In this review, we consider wedge disclinations as the main structural defects in 2D graphene crystal hexagonal lattice. Disclinations are associated with improper carbon rings, *i.e.* rings having 4, 5, 7 or 8 members to the contrary of proper 6-member carbon rings constituting ideal 2D graphene crystal lattice. With the help of disclinations, we build the models for grain boundaries (GBs) and other interfaces in graphene polycrystals as well as for pseudo-graphenes (PGs). The pseudo-graphenes are treated as graphene crystals with high density of periodically distributed disclinations with zero total charge. The geometry and energy of disclinated graphene configurations are analyzed with the help of molecular dynamics (MD) simulation technique and in the framework of the theory of defects in elastic continuum. We demonstrate that the energy of the modeled graphene interfaces reaches the value of 2 eV/Å. For symmetric tilt grain boundaries in graphene the energy stays below 0.5 eV/Å when the boundaries are in so-called equilibrium state. In the case of transition of a grain boundary to non-equilibrium state, the energy of the boundary can be up to three times higher. For investigated pseudo-graphenes, there is substantial energy excess in comparison to conventional graphene; the found energy excess can be of the order of 1 eV per carbon atom. In conclusion, it is argued that studying the properties of disclinations in graphene opens a new direction in graphene science and technology — graphene defect engineering.

Keywords: graphene, disclination, proper and improper carbon ring, grain boundary, disclination quadrupole, molecular dynamics, pseudo-graphene, disclination network.

1. Theoretical description and observation of defects in graphene

1.1. Pristine graphene and its properties

Graphene is one of the most interesting and groundbreaking discoveries of XXI century [1]. It opened the era of two-dimensional (2D) crystalline objects, which now include graphene, monolayer MoS_2 [2], hexagonal boron nitride [3], phosphorene [4], *etc.* Graphene exhibits properties of a semimetal where electron transport is essentially governed by Dirac (relativistic) equation [5]. Because of this graphene demonstrates ambipolar field effect [1] and the quantum Hall effect at room temperature [6,7]. The mechanical [8,9] and electronic [6,7,10–12] properties of graphene crystals are outstanding. This can be explored for the invention of new type electronic and optoelectronic devices [13–17]. In the process of graphene fabrication and treatment, it is practically impossible to avoid the appearance of structural defects. It is commonly known that in conventional 3D crystals the following types of defects can be distinguished [18]: 0D defects — point defects, *e.g.* vacancies and impurity atoms, 1D defects — linear chains of point defects, dislocations and disclinations; 2D defects — various interfaces including grain boundaries, twin boundaries, stacking faults, and cracks; 3D defects — voids and inclusions. In 2D crystals, we can find similar defects having one unit lower dimensionality. This review is devoted to the analysis of the properties of disclinations in graphene with special attention to their ensembles.

1.2. Evidence of defects in graphene

Vacancies, divacancies and impurity atoms. Single vacancy is a structural defect, which is formed by removal of atom in otherwise perfectly ordered crystal. As we know, pristine graphene has hexagonal lattice formed of 6-member carbon rings with sp^2 hybridization of electrons in covalent bonds [1]. We define such atomic arrangement as the configuration consisting of proper carbon rings. Then improper carbon rings will be the rings with wrong number of carbon atoms in a single ring. In graphene, vacancy, which results from one carbon atom removal in pristine lattice, evolves to a relaxed configuration consisting of neighboring 5- and 9-member carbon rings (see Fig. 1), that was confirmed in the direct *in situ* experiments [19]. We will describe the atomic configuration peculiar to a defect giving the nomenclature for the constituting defect improper rings. For example, vacancy in graphene will be designated as the configuration 5-9.

Defects in graphene can be examined exploring electron microscopy methods. Here we provide and discuss schematics of atomic configurations for graphene with

defects based on experimental data available in the literature. Divacancy defect in graphene can lead to 555-777, 5555-7777 or 5-8-5 configurations of improper rings, as it is shown in Fig. 2. In graphene, one can also experimentally observe multivacancies, *i.e.* complexes of vacancies [20]. Vacancies and their complexes serve as the centers of attraction of the impurity atoms and migration paths for carbon atoms [20,21].

Foreign atoms or molecular groups can be attached to graphene sheets leading to the functionalization of graphene [21]. In our review, we focus on structural defects consisting only of 2D and flat arrays of carbon atoms. In the case of interstitials, carbon atoms can be incorporated in graphene lattice in two ways, see Fig. 3. The pair of interstitial atoms may form so-called inverse Stone-Wales defect, see Fig. 3c.

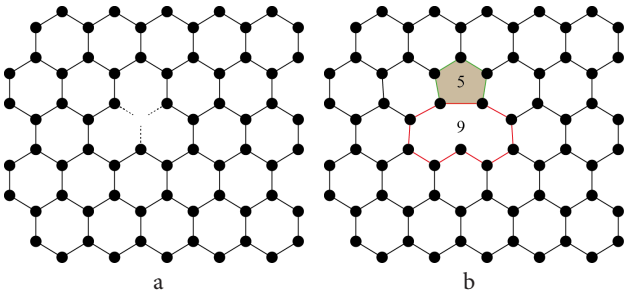

Fig. 1. Representation of a single vacancy in graphene in the form of atomic configuration made of 5- and 9-member improper carbon rings: ideal graphene lattice with removed single carbon atom (a); vacancy after reconnection of broken atomic bonds and relaxation (b). *Schematics according to experimental data from Ref. [19].*

Disclinations and dislocations. Isolated improper carbon rings in graphene can be viewed as wedge disclinations [23 – 25]. In Section 2, we consider disclination approach to graphene in details. Here we only mention that, for example, isolated 5-member improper carbon ring indicates the presence of positive wedge disclination of strength (charge) $\omega = +\pi/3$ (Fig. 4a) and isolated 7-member improper ring gives rise to negative wedge disclination with strength (charge) $\omega = -\pi/3$ (Fig. 4b) [23]. It is possible to construct dipoles of disclinations consisting of positive and negative counterparts, *e.g.* 5-7 configurations (Fig. 4c). Such dipoles are equivalent to edge dislocations in otherwise ideal graphene lattice. It is important to note the presence of distorted proper carbon rings surrounding disclinations; this is the indication of elastic fields of defects in graphene.

It can be seen from the above that improper carbon rings and their groups constitute various defects in graphene: disclinations, dislocations, and point defects. For example, 5-8-5 configuration is made of three disclinations: two positive disclinations with $\omega = +\pi/3$ and one negative disclination with $\omega = -2\pi/3$; at the same time, 5-8-5 configuration is a dislocation dipole or divacancy. The Stone-Wales defect, which formed by rotating a chain of two neighboring carbon atoms by 90° [26], is the 5-77-5 improper ring configuration (Fig. 5).

Interfaces. Interfaces in pristine graphene exist in the form of chains of improper carbon rings as it is shown in Fig. 6 [27 – 29]. We subdivide graphene interfaces into two classes: nonmisorientation interfaces (NMIs) [28] (Fig. 6a) and grain boundaries (GBs) [27,29]. In their turn, GBs can be symmetric and nonsymmetric ones. Symmetric GBs lies along a straight line (Fig. 6b). Nonsymmetric GBs possess wavy shape [27] (Fig. 6c). In the case of symmetric GBs or NMIs, one must obey special conditions for graphene growth and carefully select the substrate. Authors of Ref. [28] describe NMI consisting of 5-8-5 improper rings chain (Fig. 6a). The contact of two graphene sheets, which are grown from two crystallization centers, leads to the symmetric GB shown in Fig. 6b.

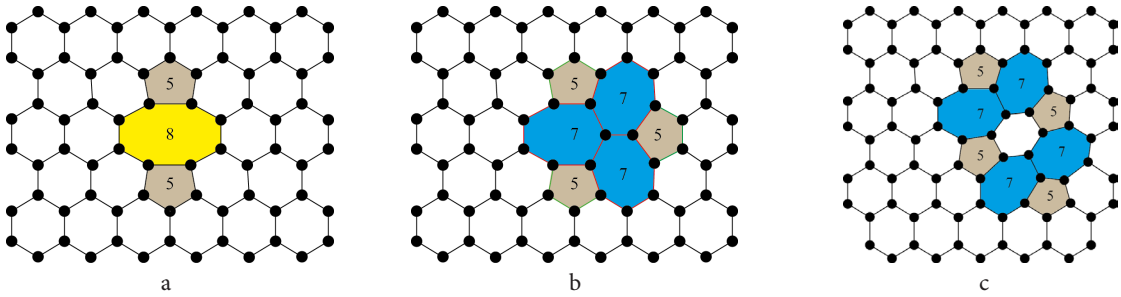

Fig. 2. Atomic configurations associated with divacancies in graphene. Configurations made of improper carbon rings: 5-8-5 (a), 555-777 (b), 5555-7777 (c). *Schematics according to experimental data from Ref. [22].*

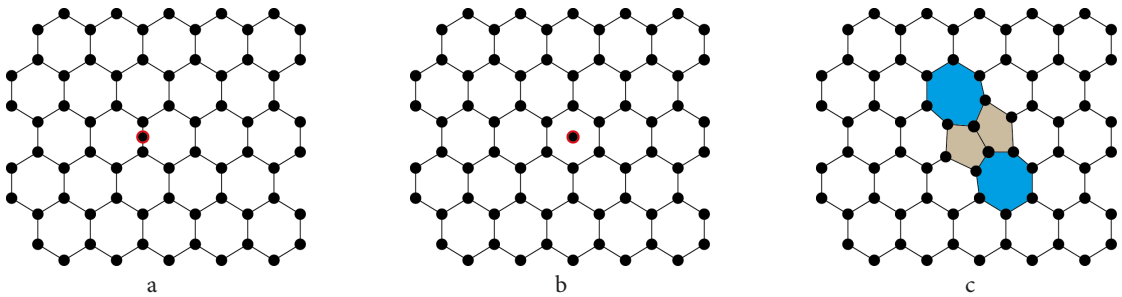

Fig. 3. Possible variants of the incorporation of extra carbon atoms in graphene lattice: bridge configuration (a); central configuration (b); the inverse Stone-Wales defect, *i.e.* 7-55-7 carbon ring configuration (c). *Schematics in (c) according to experimental data from Ref. [22].*

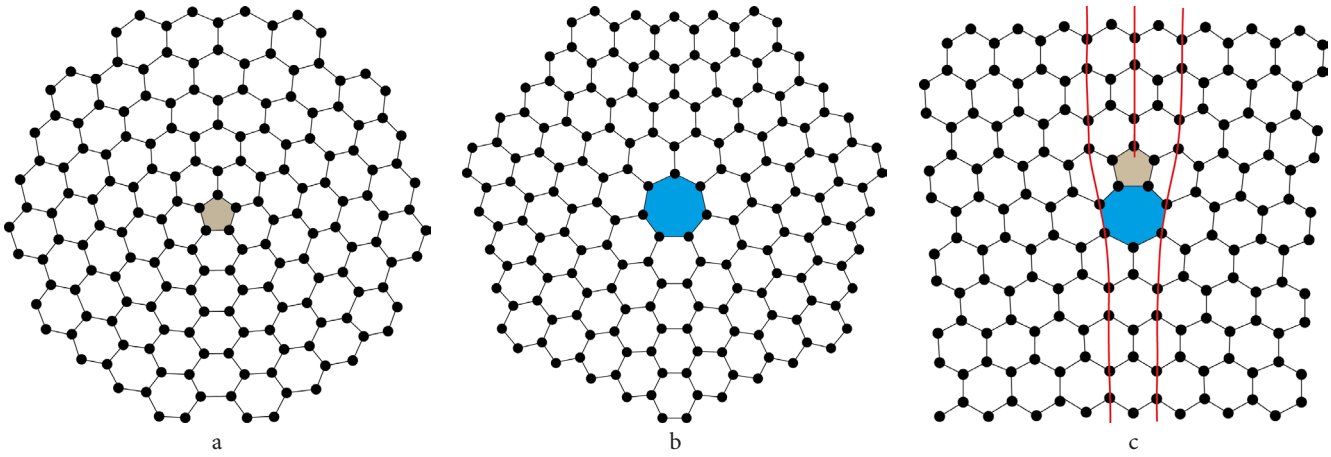

Fig. 4. Disclinations and dislocation in graphene. Disclinations of strength $\omega = +\pi/3$ (a); disclinations of strength $\omega = -\pi/3$ (b); single edge dislocation, *i.e.* 5 – 7 carbon ring configuration (c). *Schematics in (c) according to experimental data from Ref. [22].*

Graphene lattice rearrangements also take place at the edges of graphene sheets [30,31]. In this case, 5-member and 7-member improper carbon rings appear, thus constituting another type of 1D defect in 2D graphene lattice, *i.e.* graphene free edge.

Nucleation of defects during graphene processing. Defects in graphene crystals can be caused both by imperfections of the substrate, on which graphene is deposited, and by nonequilibrium conditions of the growth process [28,32]. Growth of graphene at high temperatures allows defect annealing [33]. On the other hand, at low-temperature growth, defect formation becomes a serious problem [32,34]. The bombardment of graphene by electrons or ions initiates point defect formation. This process eventually leads to the formation of pores of a certain diameter in the graphene sheets [35].

1.3. Approaches to modeling graphene with defects

MD simulations. Molecular dynamics (MD) is computer simulation method for investigating the evolution of atomic and molecular structure in time and space. Molecular dynamics solves the system of equations of motion. These equations of motion are essentially Newton's second law. The implementation of this method requires the definition of potential function — interatomic potential. A simplest example of interatomic potential is Lennard-Jones potential, also termed as the «6-12 potential». There is a large amount of potentials used for various materials and models. To investigate carbon based including graphene, one usually utilizes AIREBO [36] or Tersoff [37] potential functions. For studying of a graphene in contact with other materials, one can apply co-called semi-empirical potentials or universal Lennard-Jones potential [38].

In our own implementation of MD technique to graphene structures, we used AIREBO potential. We also imposed

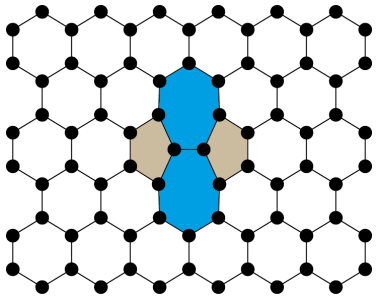

Fig. 5. Stone-Wales defect, *i.e.* 5-77-5 carbon ring configuration. *Schematics according to experimental data from Ref. [19].*

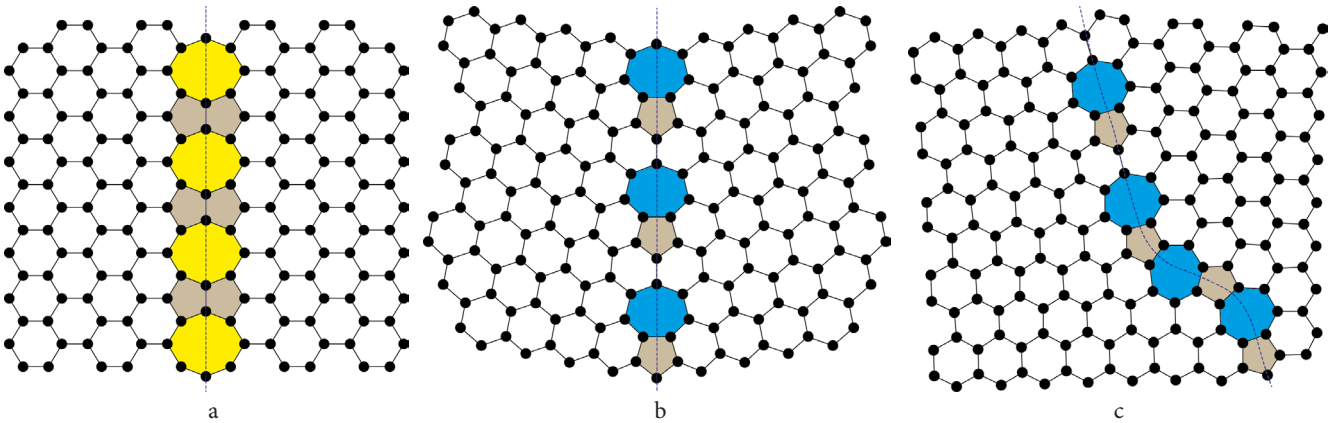

Fig. 6. Examples of interfaces in graphene: no misorientation interface — chain of 5-8-5 carbon rings (a), symmetric (b) and nonsymmetric (c) grain boundaries. *Schematics in (a) and (c) according to experimental data from Refs. [28] and [27], respectively.*

a restriction on the exit of the carbon atoms to the third dimension, *i.e.* we considered essentially flat 2D systems. The MD simulation was performed at 0 K with the periodic boundary conditions.

DFT simulations. Density functional theory [39] is a computer quantum mechanical method to investigate the electronic structure of materials. The properties of a system can be determined by using functionals of the electron density. For graphene study, one usually uses the generalized gradient approximation functional of Perdew, Burke and Ernzerhof (GGA PBE) [40].

Elastic theory analysis. Theory of elasticity helps when analyzing graphene structures within continuum approximation [41]. Exploring elasticity approach one derives analytical formulas for energies of disclinations and their ensembles in graphene. An important starting point in continuum mechanics modeling is the choice of nomenclature and geometrical scheme for defects under consideration. Then, the equations of 2D isotropic elasticity are used to find elastic fields and energies of disclination ensembles in graphene [41,42].

2. Isolated defects in 2D crystals

2.1. Disclinations in 2D hexagonal crystals

The procedure of the creation of an isolated improper carbon ring in a finite size graphene sheet is given schematically in Fig. 7.

This procedure, which also known for 3D solids as Volterra process, see, *e.g.* [42], for wedge disclination formation, operates with the removal/insertion of the wedge of material after cutting along a line (plane in case of 3D) of the sheet [23]. As a result, single wedge disclination localized in the position of improper carbon ring elastically distorts the overall graphene sheet and change the external shape of the sheet and its symmetry. The presence of the positive wedge disclination of strength (charge) $\omega = +\pi/3$ (Fig. 7a) leads to 5-fold symmetry, whereas the presence of negative wedge disclination of strength (charge) $\omega = -\pi/3$ (Fig. 7b) — to 7-fold symmetry.

Basing on such an equivalence between improper carbon rings in graphene and disclinations we can apply elasticity of disclinations for analyzing properties of defects in graphene including their self and interaction energies. In particular, simple expression for the energy E of the wedge disclination in the center of elastically isotropic disk [42,43] is of great importance:

$$E = \frac{G(1+\nu)}{16\pi}\omega^2 R^2, \qquad (1)$$

where ω is the strength of the disclination, G is the shear modulus in units [*Force/Length*], ν is Poisson ratio, R is the radius of the disk. From Eq. (1) it follows that the energy of an isolated disclination in graphene sheet scales quadratically with its size leading to enormous large values and making impossible the existence of such defects in real physical objects.

Disclinations in solids are realized in the form of self-screening ensembles, *i.e.* dipoles and quadrupoles [42,43]. As it will be shown below in Sections 3 and 4, in graphene, self-screening ensembles of disclinations form dipole and quadrupole chains contributing to the structure and properties of grain and intercrystallite boundaries, or periodic distributions giving rise to pseudo-graphenes.

To find the energies of disclination ensembles in graphene in the framework of the analytical approach one can use the results of Refs. [41,44] for energy E_N of N disclinations in an elastic disk. In Fig. 8, the geometrical scheme for calculation of energy E_N is shown. In such a geometry E_N is expressed by the following formula:

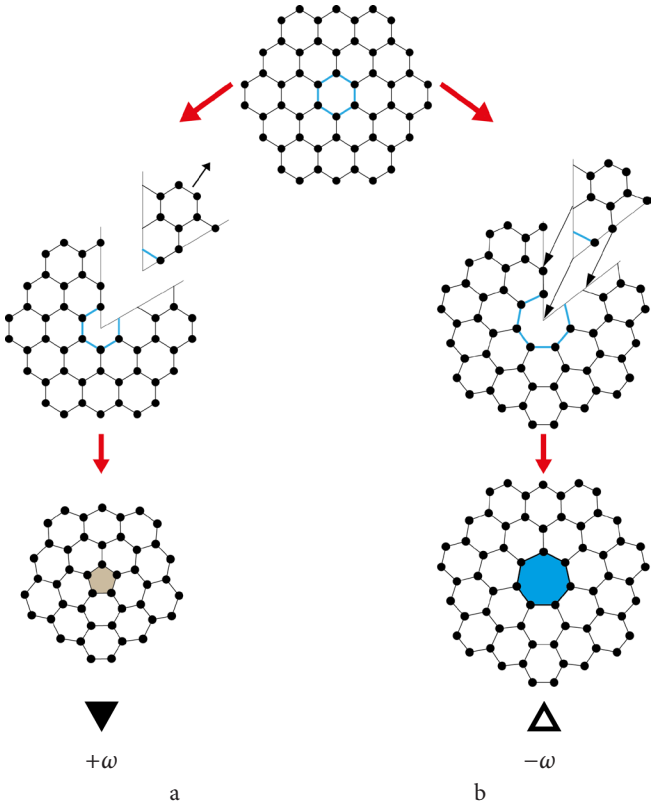

Fig. 7. Volterra procedure for the formation of wedge disclinations in 2D hexagonal crystal lattice: positive disclination and associated 5-member ring (a) and negative disclination and associated 7-member ring (b). Minimal magnitude of disclination strength in hexagonal lattice is $\omega = \pi/3$. Positive and negative disclinations are denoted by black and empty triangles, respectively [23].

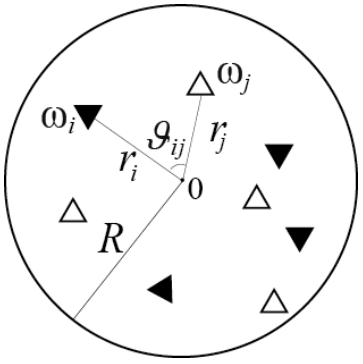

Fig. 8. Schematics for calculating energy of the disclination ensemble in an elastic disk [41].

$$E_N = \frac{G(1+\nu)}{8\pi}\left(\sum_i^N \frac{\omega_i^2 R^2}{2}\left(1-\frac{r_i}{R}\right)+\sum_{i=1}^N\sum_{j=i+1}^N \omega_i\omega_j \cdot\right.$$
$$\cdot\left[\left(r_i^2+r_j^2-2r_i r_j\cos\upsilon_{ij}\right)\log\frac{R^2(r_i^2+r_j^2-2r_i r_j\cos\upsilon_{ij})}{r_i^2 r_j^2-2R^2 r_i r_j\cos\upsilon_{ij}+R^4}+\right. \quad (2)$$
$$\left.\left.+R^2-r_i^2-r_j^2+\frac{r_i^2 r_j^2}{R^2}\right]\right),$$

where ω_i is a strength of the *i*- disclination; r_i is a distance between center of disk and *i*-disclination; υ_{ij} is an angle between radiuses of *i*- and *j*- disclinations; *R* is a radius of the disc. In Eq. (2) we take into account that the disk is infinitely thin, *i.e.* is a 2D solid.

2.2. Classification of defects in 2D elastic continuum

To date, clear and direct method for modeling defects is based on the concept of the *eigenstrain*, which was first proposed by Eshelby for elastic inclusions [45]. *Eigenstrain* tensor is a complete characteristic of the defect. It shows "how" and "where" a defect is specified in an elastic medium. The response of an elastic medium to a given *eigenstrain* determines uniquely the elastic fields of the defect. With the help of the well-developed mathematics, the elastic fields generated by defect can be found from its *eigenstrain* [46].

The foundation of *eigenstrain* is based on the following Eshelby procedure: a cut is made in an elastic body, the material is removed, and then subjected to change of the shape, which is due to stress-free strain, *e.g.* plastic deformation or strain associated with phase transformation. Forces are applied to this deformed volume of material in order to insert it into the original configuration exactly at the place of the cut, then, the surfaces of the cut are glued together and the forces are removed.

The Eshelby procedure applied to regions of different dimensions leads to defects of different dimensions. Consequently, we can introduce a classification of defects in an elastic medium, based on the dimension *n* of the region Ω_n of *eigenstrain* ${}^n\varepsilon_{ij}^*$ or *self-distortion* ${}^n\beta_{ij}^*$ [47,48]. Note that ${}^n\varepsilon_{ij}^*$ is symmetrized ${}^n\beta_{ij}^*$.

In 2D elastic media, defects can be subdivided into three classes.

Point defects ($n=0$)**.** The elementary point defects are the infinitesimal dislocation loops in both the 2D and 3D media [49]. In the *xy*-plane film, the self-distortion of the infinitesimal dislocation loop becomes:

$${}^0\beta_{ij}^* = -b_j l_i \delta(\mathbf{r}-\mathbf{r}_0), \quad i,j=x,y, \quad (3)$$

where b_j is the dislocation Burgers vector; $\mathbf{r}_0$ is the coordinate of the loop on the *xy*-plane, l_i is the segment, which is an analog of the area s_i for an infinitesimal dislocation loop in the 3D medium, $\delta(\mathbf{r}-\mathbf{r}_0)$ is the two-dimensional Dirac delta function, given by the relation $\delta(r-r_0)=\delta(x-x_0)\,\delta(y-y_0)$.

Two mutually perpendicular infinitesimal dislocation loops form a dilatation center with the following *self-distortion*:

$${}^0\beta_{ii}^* = bl\delta(\mathbf{r}-\mathbf{r}_0) = \tfrac{1}{2}\Delta s\,\delta(\mathbf{r}-\mathbf{r}_0), \quad i,j=x,y, \quad (4)$$

where *l* is the initial linear size of the loop, $b=\Delta l$ is the change in the linear size, $\Delta s=(l+\Delta l)^2-l^2\approx 2l\Delta l$.

With a formal approach, the self-distortion of a point defect in a 2D medium can be written:

$${}^0\beta_{ij}^* = \beta_{ij}^* s\,\delta(\mathbf{r}-\mathbf{r}_0), \quad i,j=x,y, \quad (5)$$

where *s* is a formal dimensional factor.

One-dimensional defects ($n=1$)**.** The *self-distortion* of any one-dimensional defect located, for example, on a segment $[y_1, y_2]$ having a coordinate x_0, reads:

$${}^1\beta_{ij}^* = \beta_{ij}^* l\,\delta(x-x_0)H(y_1\le y\le y_2), \quad (6)$$

where β_{ij}^* is the *self-distortion* of the line segment; *l* is a linear factor, $H(y_1\le y\le y_2)$ is the Heaviside function.

In 2D media, the Somigliana dislocations are one-dimensional defects, and the Volterra dislocations and disclinations are *degenerate* one-dimensional defects [47,48]. Degeneration means that in a 2D crystal, complete (perfect) Volterra dislocations and disclinations look like point defects.

We can rewrite the *self-distortion* of the dislocation in the form typical for Volterra dislocations, *i.e.* via Burgers vector [47, 48]:

$$\begin{aligned} {}^1\beta_{xx}^* &= -b_x\delta(x-x_0)H(y_0\le y\le\infty) \\ {}^1\beta_{yx}^* &= -b_x\delta(x-x_0)H(x_0\le x\le\infty). \end{aligned} \quad (7)$$

A linear defect can be represented through point defects continuously distributed with some linear density along a line.

Two-dimensional defects ($n=2$)**.** The area of determining the *eigenstrain* or *self-distortion* of two-dimensional defects is a part of the surface. In a 2D medium, two-dimensional defects are similar to inclusions in a 3D medium.

In general, for a two-dimensional defect in the film, we can write:

$${}^2\beta_{ij}^* = \beta_{ij}^*\delta(S_{incl}). \quad (8)$$

Here $\delta(S_{incl}) = \begin{cases} 1, & \mathbf{r}\in S_{incl} \\ 0, & \mathbf{r}\notin S_{incl} \end{cases}$.

A two-dimensional defect can be also represented through distribution of point defects over the surface S_{incl}.

It is worth noting that in a 2D continuum, defects of dimension lower than 2 are described by *eigenstrains* (*self-distortions*), which contain some arbitrary dimensional factors, see Eqs. (5) and (6), as is the case with defects of dimension lower than 3 in a 3D medium.

In 2D flat elastic media, using the Green function ${}^2G_{ij}$ and elastic modules C_{jklm} the *eigenstrain* ${}^n\varepsilon_{ij}^*$ (or *self-distortion* ${}^n\beta_{ij}^*$) allows to find the total displacement field of a defect [46]:

$$u_i^t(\mathbf{r}) = -\int_{S'} C_{jklm}\,{}^n\varepsilon_{km}^*(\mathbf{r}')\,{}^2G_{ij,l}(|\mathbf{r}-\mathbf{r}'|)\,dS', \quad (9)$$

where the left upper index 2 in Green function indicates the dimension of the medium.

For the isotropic elastic medium, the Green function ${}^2G_{ij}$ and the elastic modules C_{jklm} are [46]:

$${}^2G_{ij}(|\mathbf{r}-\mathbf{r}_0|) = \frac{1}{8\pi(1-\nu)G}\left\{\frac{(x_i-x_i')(x_j-x_j')}{\bar{r}^2}-(3-4\nu)\delta_{ij}\ln\bar{r}\right\}, \quad (10a)$$

$$C_{jklm} = \frac{2G\nu}{1-2\nu}\delta_{jl}\delta_{km}+G(\delta_{lk}\delta_{jm}+\delta_{lm}\delta_{jk}), \quad (10b)$$

where $\overline{r}^2=(x-x')^2+(y-y')^2$, δ_{km} is the Kronecker delta, G is the shear modulus, and ν is the Poisson ratio.

Since in our case the elastic space is a 2D layer with free surfaces, which lies in the xy-plane, the stress tensor does not contain the components σ_{zj}. This means that we deal with the plane stress state and hence in both the Green function and Hooke law, the Young modulus E and the Poisson ratio ν should be replaced by ratios $E(1+2\nu)/(1+\nu)^2$ and $\nu/(1+\nu)$, respectively [46]. Since the shear modulus $G=E/[2(1+\nu)]$, the replacement procedure does not affect it. In the transition from the 3D case to the 2D case, the unit of measurement of the Young and shear moduli change from [N/m^2] to [N/m].

For the first time, by using Eqs. (9) and (10a, b) and *self-distortion* Eq. (3) the elastic fields of an infinitesimal prismatic dislocation loop was calculated [47,48]. Also, it was found that the elastic fields due to dilatational center in 2D medium precisely coincide with the fields caused by a biaxial dilatation line in the 3D medium when replacing ν by $\nu/(1+\nu)$ [47,48,50].

It is clear that defects causing a plane strain in a 3D medium have their counterparts of smaller dimension in the film. Straight-line edge dislocations and wedge disclinations in 3D media generate plane strain states, see, for example, [42,51]. Therefore, the main difference between the stress fields of these defects in a film and in an infinite 3D medium is the absence of the σ_{zz} component. The other stress components of dislocations and disclinations coincide with the accuracy to the factors associated with Poisson ratio ν.

Earlier, in Refs. [52, 53], the solutions of the boundary-value problems for edge dislocations and wedge disclinations perpendicular to the free surfaces of a plate having a finite thickness were presented. In particular, it was shown in Ref. [52] that when the plate thickness tends to zero, the elastic field generated by the edge dislocation becomes as that in the plane stress state. In this regard, the fields of the edge dislocations and wedge disclination in the 3D medium can be transform to those of their counterparts in the 2D crystal by the change in elastic moduli as noted above.

As can be seen from Figs. 6a–c and will be explained below, the disclination dipole is a characteristic element of grain boundaries in graphene. Using the rows of disclination dipoles with their elastic fields it is possible to calculate the strain energy of GBs in graphene without exploiting the computer simulation.

3. Modeling of interfaces in graphene

3.1. Structure of NMIs and GBs

The first step in the MD analysis of interfaces in graphene is the creation of starting atomic configurations. Interfaces can be constructed in the form of chains of disclination structural units (DSUs) — specific disclination dipoles or quadrupoles (Fig. 9) [23,54].

The application of periodic boundary conditions in MD simulation for a single GB with misorientaion is problematic. To solve this, one can simulate atomic configurations that contain two GBs with opposite misorientation. The condition of absence of influence of geometry and size of system on energy of the modelled interface must be satisfied; this means that interfaces in the graphene sheet should not interact with each other. For details on eliminating the influence of the edge of graphene sheets on the results of MD simulation, see Ref. [54].

All initial graphene configurations with DSU chains were then equilibrated in MD simulations to the reach a local energy minimum of the system. The resulting atomic configurations for a number of graphene interfaces together with their misorientation angles θ and disclination content are shown in Fig. 10.

The comprehensive list of references devoted to the structure and properties of interfaces in graphene can be found in our recent publications [23,54,55].

3.2. Energy of grain boundaries

The results of MD calculation of energies for the mentioned above graphene interfaces are presented in the chart form in Fig. 11 and listed in Table 1 [23]. The grain boundaries in graphene, consisting of 5-member and 7-member rings, were studied in a number of works, *e.g.* Ref. [56], where the dependence of graphene GB energy on grain misorientation angle θ was reported for the first time.

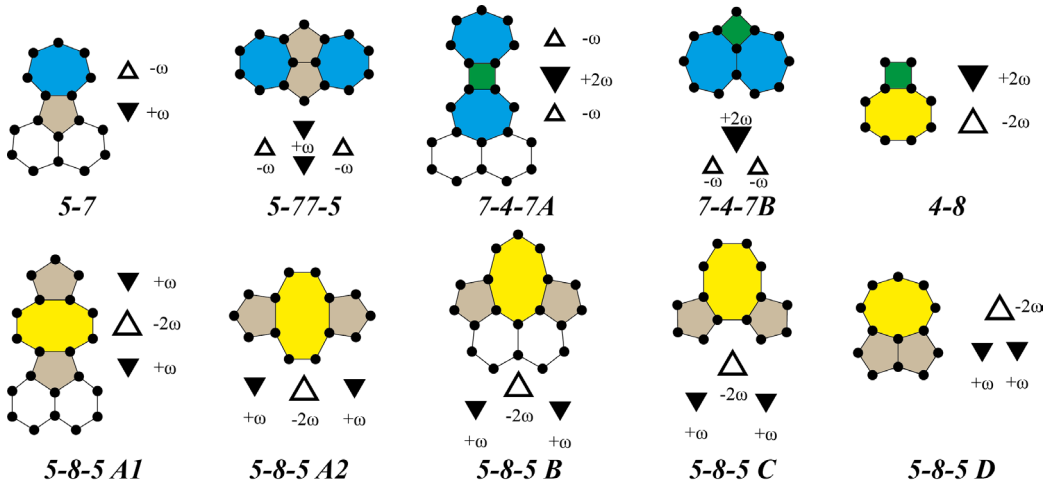

Fig. 9. Disclination structural units (DSUs) of interfaces containing 8-, 7-, 5- and 4-member improper carbon rings and the corresponding disclination schemes operating with DSUs; $\omega=\pi/3$.

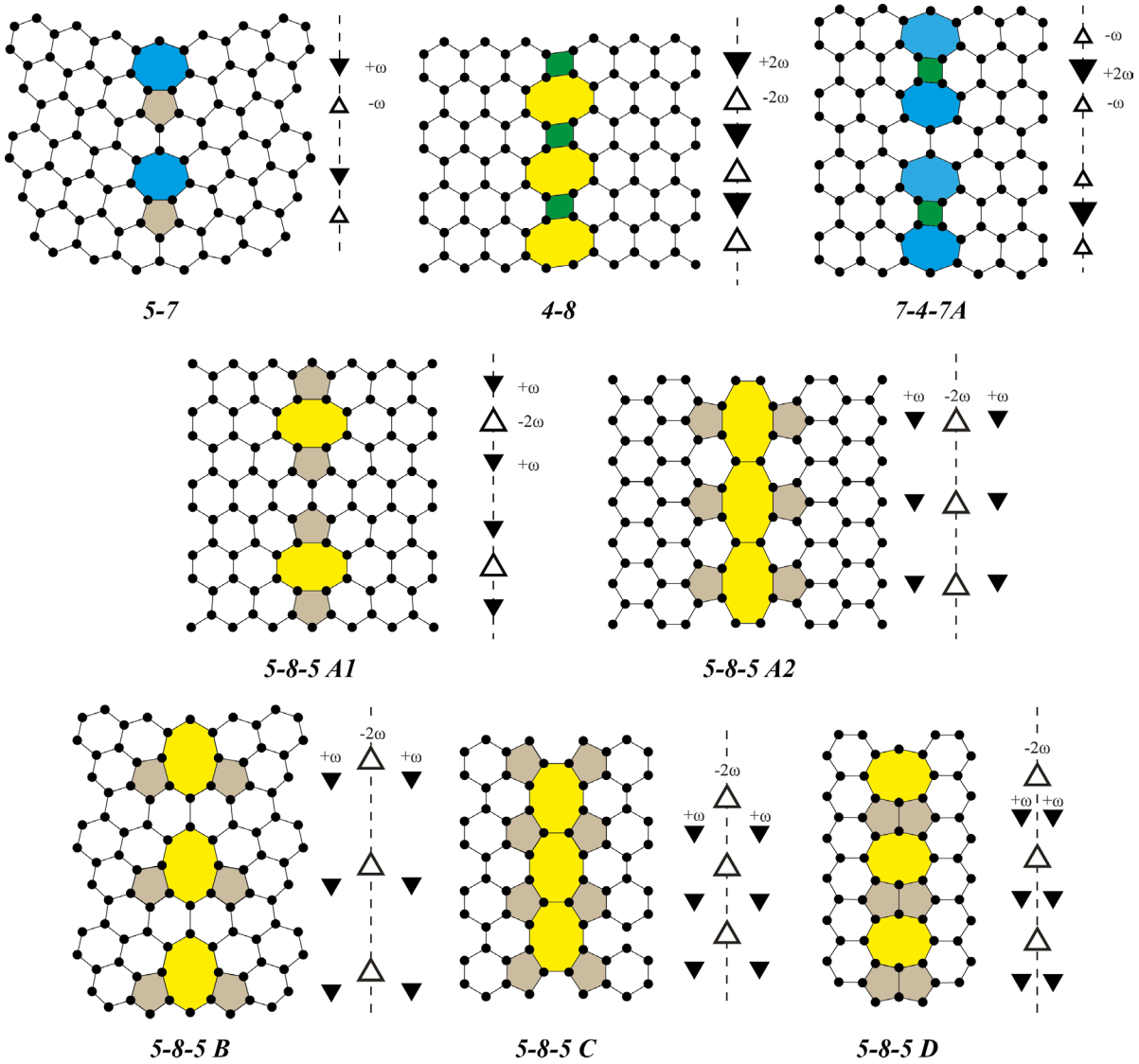

Fig. 10. Interfaces if graphene constructed with the help of DSUs shown in Fig. 9 and corresponding disclination stricture schemes; note that configurations with $\theta = 60°$ gives zero misorientation between neighboring graphene parts, each of each is however rotated by ±30° with respect to original graphene orientation.

3.3. Equilibrium and non-equilibrium GBs in graphene

The structure and energy of symmetric GBs in graphene have been investigated in details in Ref. [55], where the DSU approach was adopted to model equilibrium as well as non-equilibrium states of GBs, for which the same average misorientation holds (Fig. 12), but the GB energy varies. Initially, the DSU approach was applied to the analysis of GB in metals in Refs. [57,58].

In accordance with the DSU approach, non-equilibrium GBs in graphene were modeled as non-uniform distributions of DSUs 5-7 (see Fig. 9a), which are represented at mesoscale as disordered networks of disclination dipoles (Fig. 13).

The obtained dependence of GB energy of equilibrium GBs on misorientation angle in the whole interval $0° \le \theta \le 60°$ is substantially nonbell-shaped (see Fig. 13) that is associated with structural differences of the GBs with θ and $(60° - \theta)$ and agrees well with literature data on orientation-dependent properties of GBs in graphene [56,59]. It was demonstrated that the energy of non-equilibrium GB in graphene can substantially exceed the energy of equilibrium GB with the same misorientation angle (see Fig. 13) [55]. The energy of non-equilibrium GB is highly affected by degree of DSU distribution irregularity and lesser extent by GB average misorientation angle.

Table 1. Energies of interfaces in graphene.

Type of interface	Misorientation angle	Simulated energy per unit length, eV/Å
5-7	21.8°	0.439
5-8-5A1	0°	0.886
5-8-5A2	60°	2.253
5-8-5B	13.7°	1.408
5-8-5C	0°	1.292
5-8-5D	60°	0.639
4-8	0°	1.051
7-4-7 A1	0°	1.247

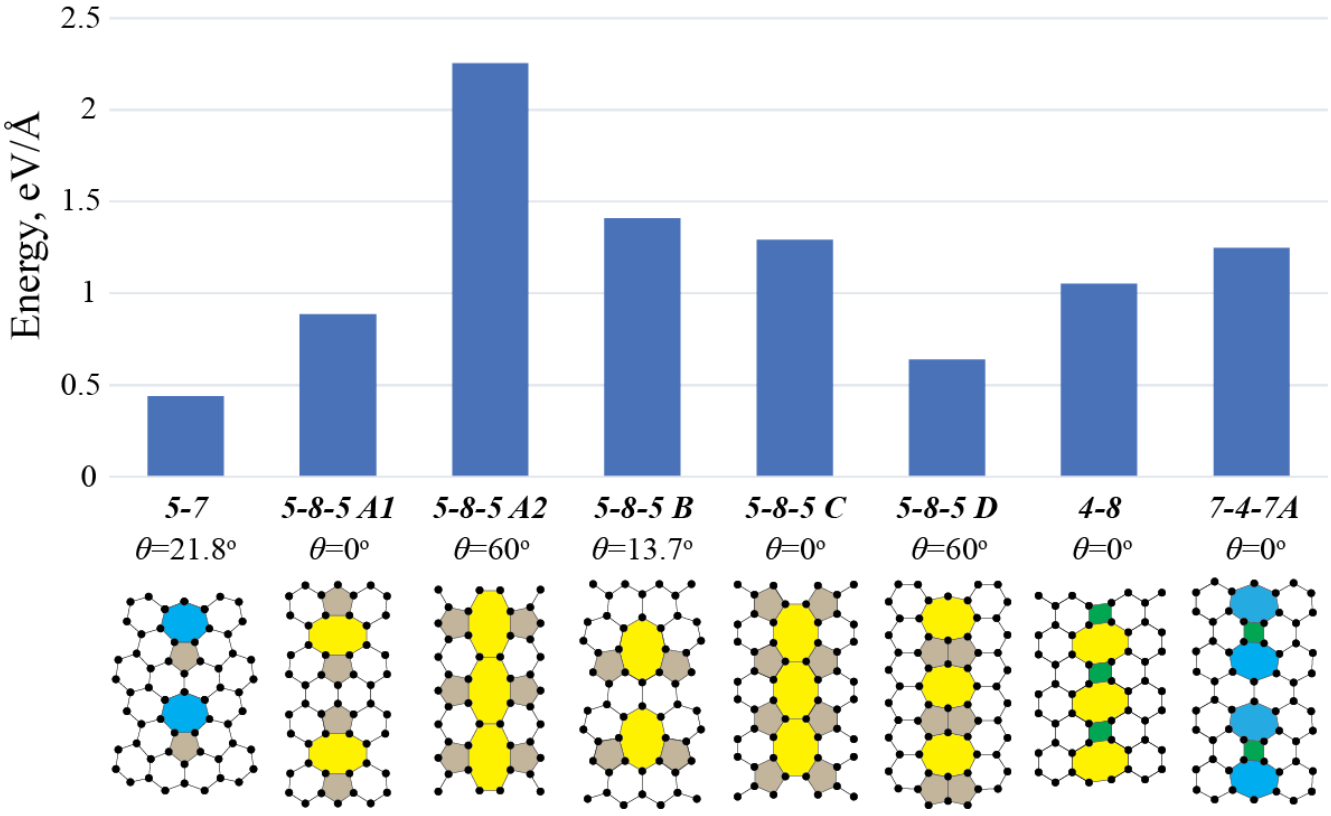

Fig. 11. Energies, misorientation and atomic structure of interfaces in graphene.

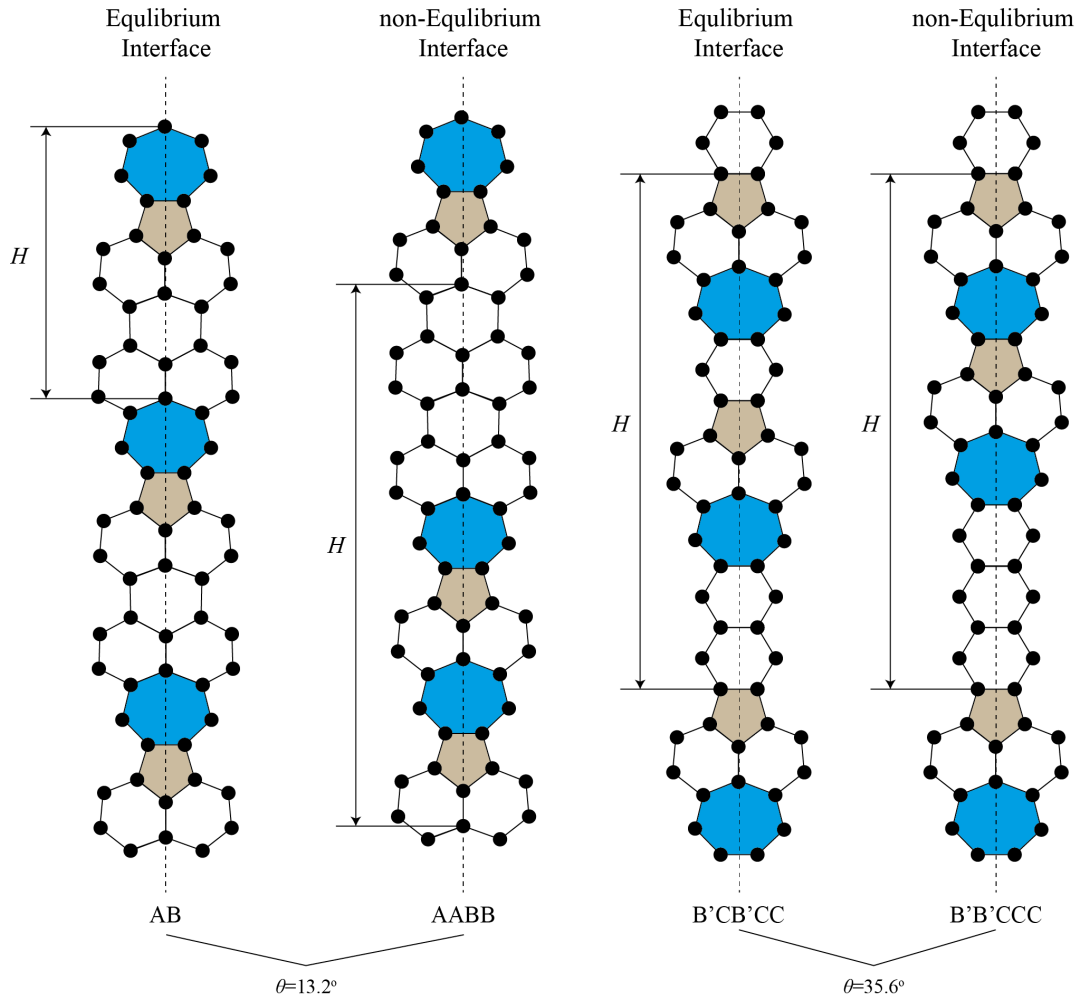

Fig. 12. Examples of equilibrium and non-equilibrium symmetric grain boundaries in graphene [55].

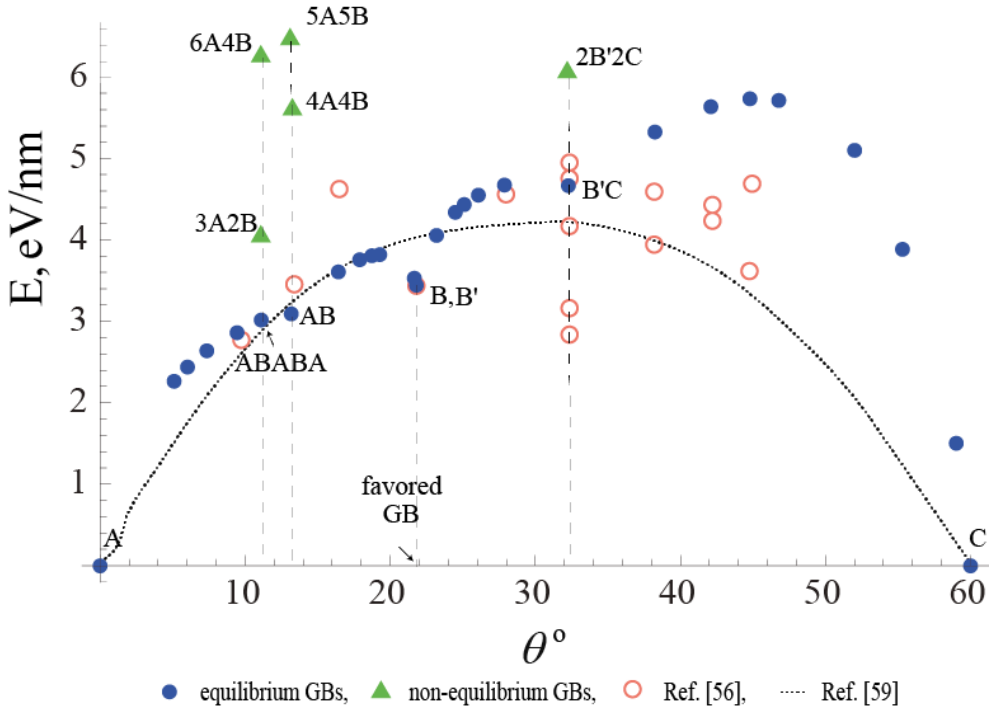

Fig. 13. Dependence of grain boundary (GB) energy on misorientation angle θ in graphene for equilibrium (filled blue circles) and non-equilibrium (green triangles) GBs [55]. Dashed line and empty red circles correspond to results from Refs. [56] and [59], respectively.

3.4. Influence of GBs on graphene properties

It was reported in Ref. [50] that symmetrical GBs composed of DSUs 5-7 create jumps of temperature at the interface that was attributed to the fact that thermal conductivity of GBs is different from those for defect-free graphene. The symmetrical NMIs composed of DSUs 5-8-5D can be considered as a «metallic wires» and may be used as a molecular membrane for selective diffusion of atoms or small molecules [28].

The dependence of mechanical properties on misorientation angle of GBs was theoretically investigated in Ref. [24], where anomalous strength behavior of graphene with tilt GBs was reported: with decreasing the misorientation angle from 30° to 5°, the fracture strength and fracture strain of graphene sheets with GBs were decreasing. The structure of graphene sheet edges influence the electronic [61, 62] and mechanical [63] properties of graphene sheet as a whole.

4. Pseudo-graphenes

4.1. Structure of pseudo-graphenes

The interfaces and GBs discussed Section 3 can be used as a structural element to create graphene-like materials with periodically distributed improper carbon rings, *i.e.* disclination defects (Fig. 14).

Graphene crystals with the densest distributions of disclinations having in their cores improper 4-, 5-, 7-, 8-member carbon rings contain a minimal number of proper 6-member carbon rings. These carbon crystals can be classified as pseudo-graphenes (PGs) (Fig. 15) [64]. Note that one of the first pseudo-graphenes, namely phagraphene (configuration 5-7 A in Fig. 15) was introduced in Ref. [65].

4.2. Energy of pseudo-graphenes

The densest distributions of disclinations in graphene lattice guarantee a minimal total energy of the structure; Ref. [64] describes this fact in detail. When close packed, disclinations of opposite sign screen elastic fields of each other forming disclination network (DN), thus reducing the stored elastic energy in graphene crystal. For example, graphene crystals with various density of uniformly distributed 4-member and 8-member improper carbon rings are presented in Fig. 16. The dependence of energy on density of defects is then given in Fig. 17. Crystal marked "4-8 g0" is PG "4-8" (Fig. 15). It follows from the diagram that, with the exception of the tightly packed structure "4-8 g0", the average energy per atom in the crystal depends weakly on the period of the DN.

On the other hand, if we consider PGs with varying density of DSUs, *i.e.* disclination quadrupoles (Fig. 18), we get another tendency; namely, the reduction in the density of DSUs (disclination quadrupoles) in material lowers its energy (Fig. 19).

Energies per carbon atom for PGs shown in Fig. 15 are summarized in the diagram in Fig. 20.

4.3. Disclination approach to pseudo-graphenes

The energy associated with the ensemble of improper carbon rings in PGs can be found with the analytical formulas of disclination approach, i.e. by exploring Eq. (2) for corresponding PG disclination configuration. To do this, the self-screened disclination ensemble should be defined for each pseudo-graphene.

The disclination ensemble becomes self-screened when its energy does not depend on the external screening parameter R. This is true for zero total disclination charge

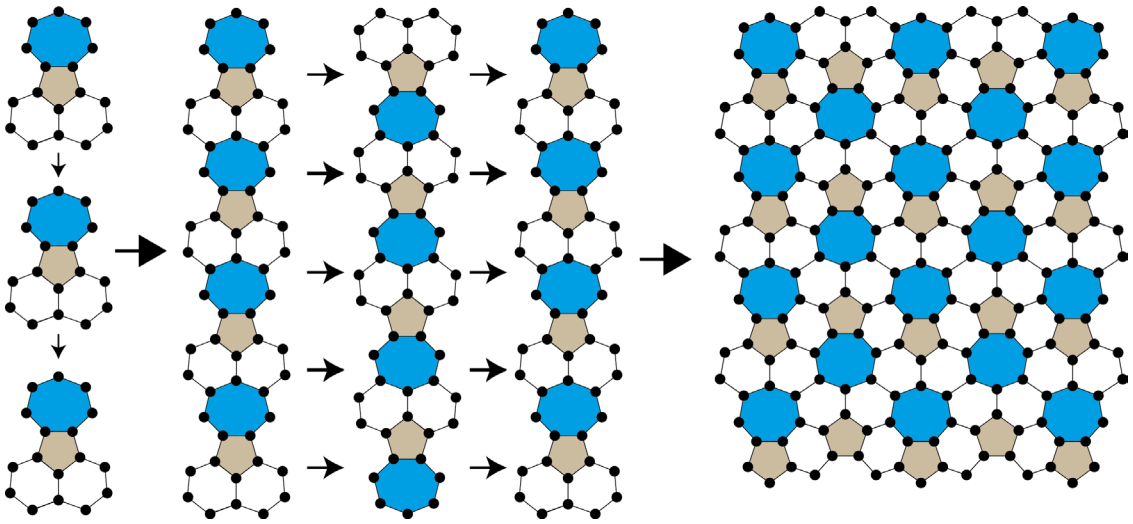

Fig. 14. Assembling of the phagraphene from GBs with DSUs 5-7.

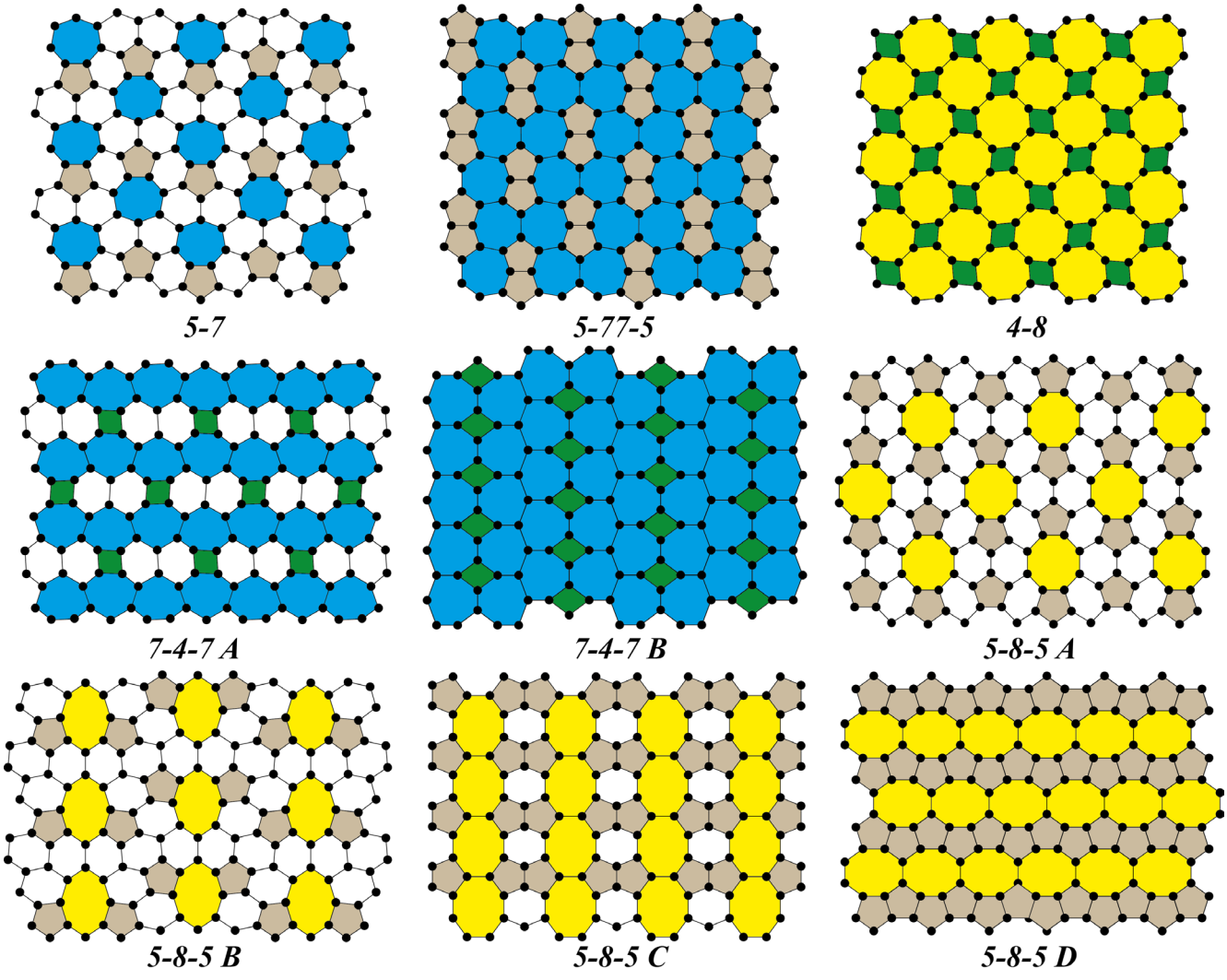

Fig. 15. Pseudo-graphene crystals (PGCs).

and zero disclination dipole moment of the ensemble of N disclinations. The simplest self-screening disclination ensembles are quadrupoles in the forms of a rectangle or line. Their energies are known, *e.g.* see Refs. [42, 43]. Additional analysis of Eq. (2) shows that the most general self-screening ensembles, *i.e.* those with the energies that does not depend on the external parameter R, are quadrupoles in the form of parallelograms and its particular cases (Fig. 21). These quadrupoles can be recognized in graphene structures as repetitive self-screening ensembles, and hence their energies should be used to calculate the energy of disclination networks E_{DN} as a whole.

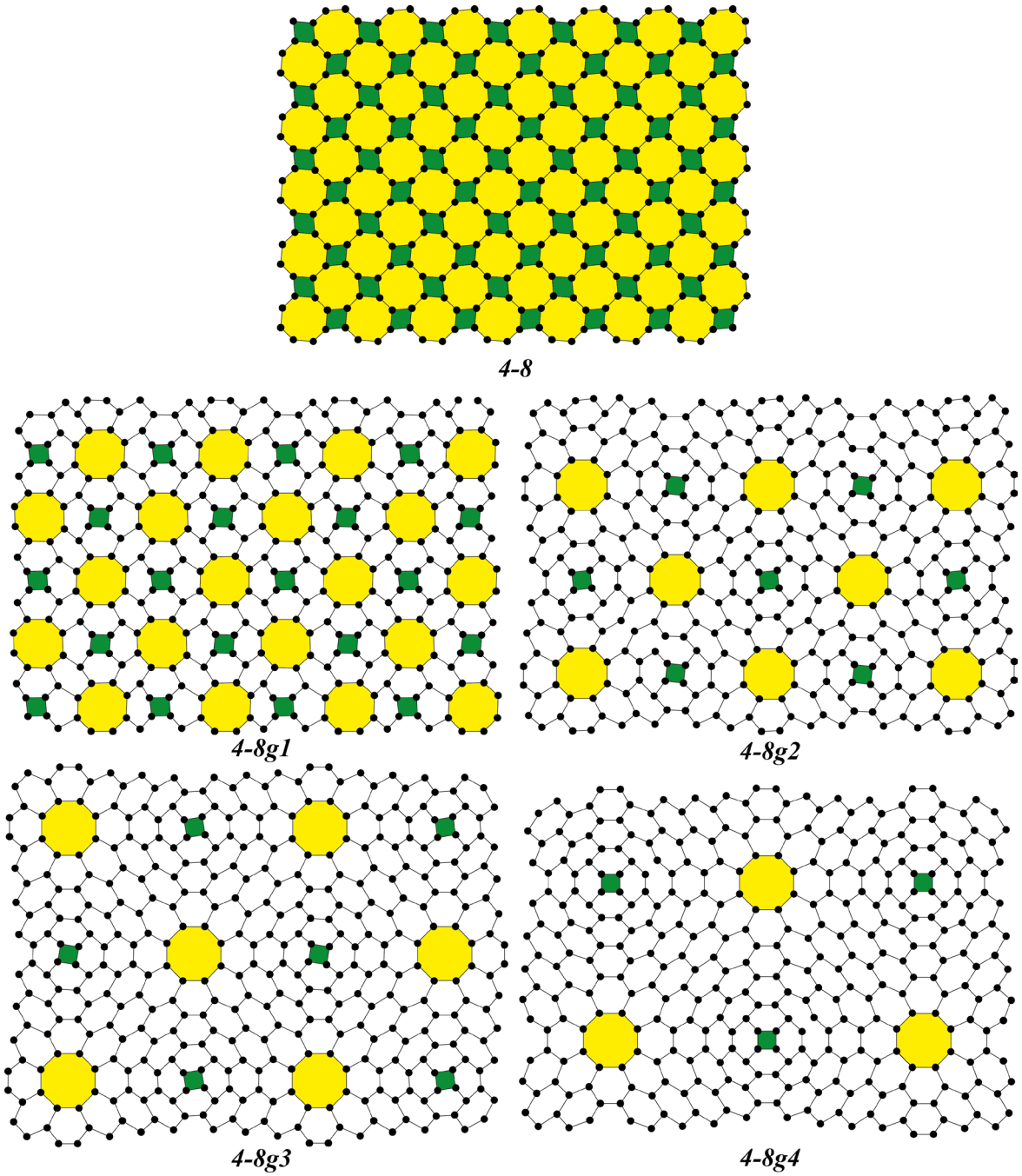

Fig. 16. Networks of improper 4-member and 8-member carbon rings in graphene as periodic structures of disclinations of strength $\omega = +2\pi/3$ and $-2\pi/3$.

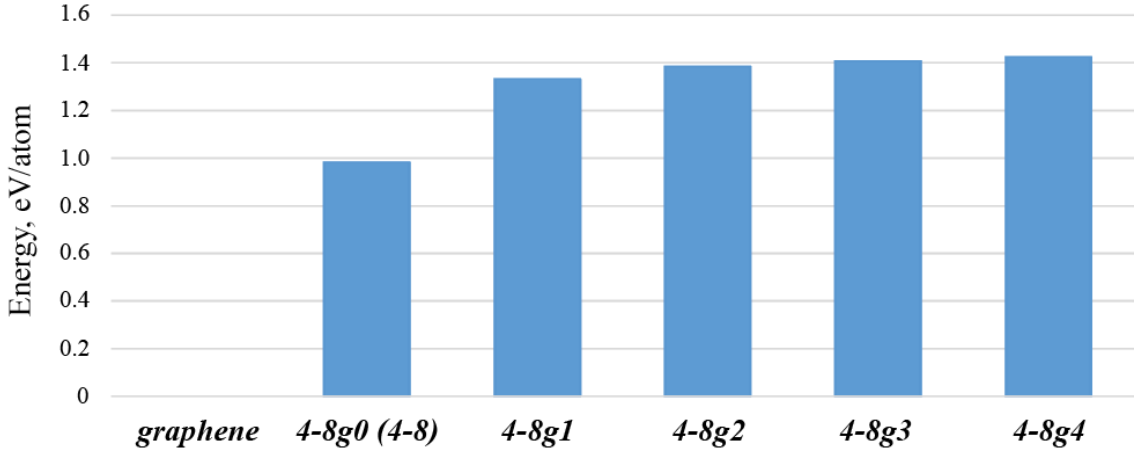

Fig. 17. Energy per carbon atom for graphene crystals with periodically distributed disclinations given in Fig. 16.

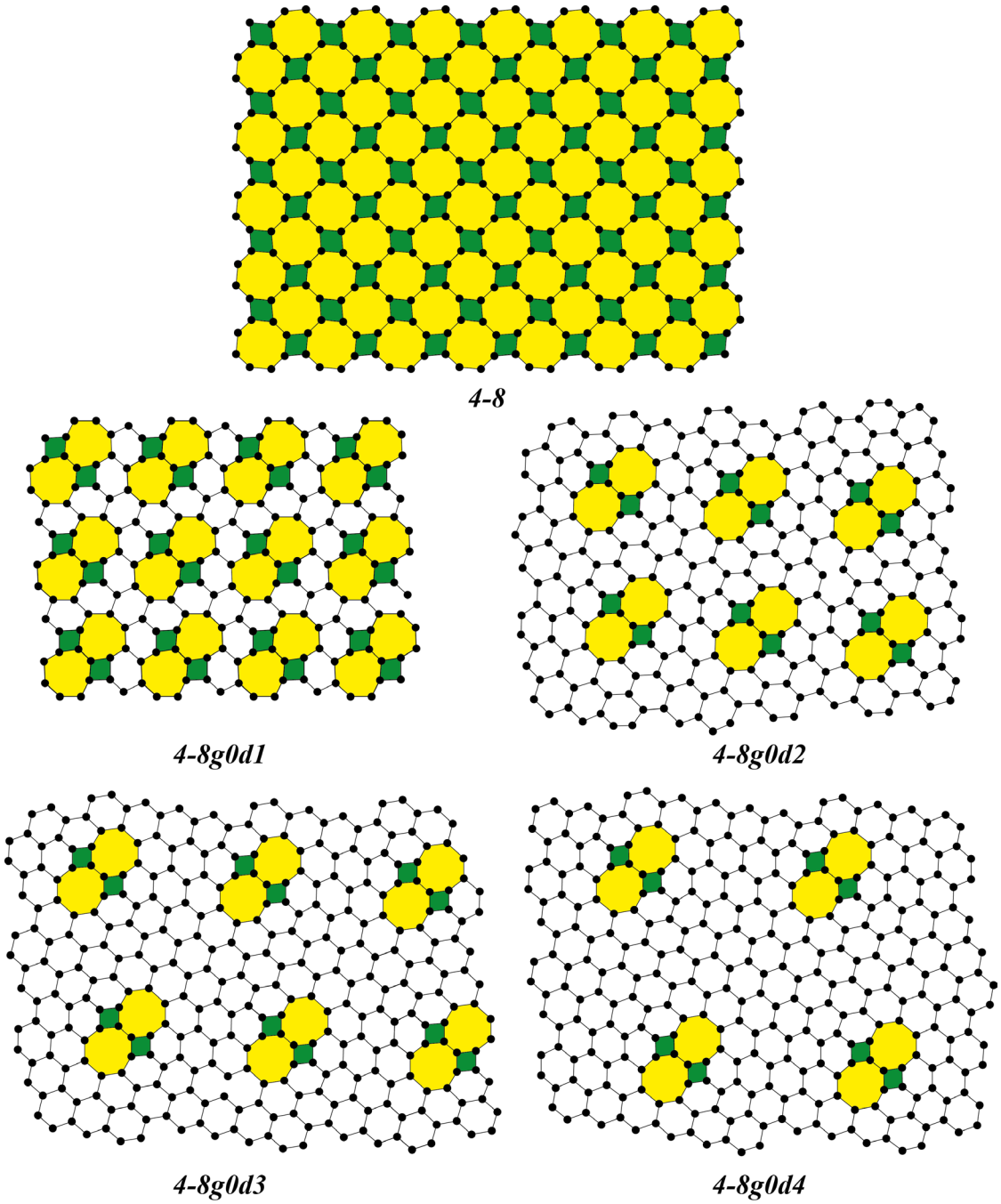

Fig. 18. Periodic networks of disclination quadrupoles in pseudo-graphenes.

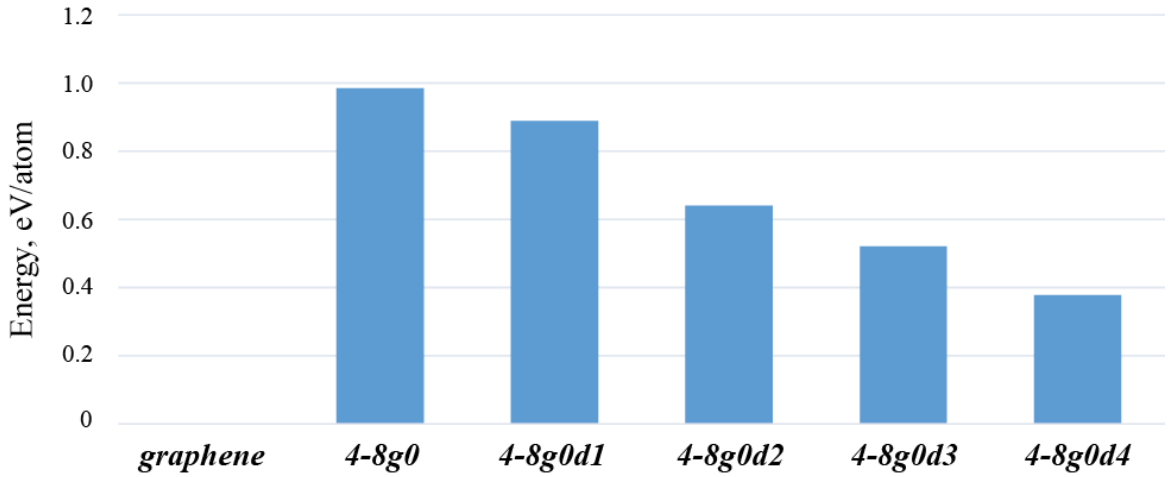

Fig. 19. Energy per atom for pseudo-graphenes with periodic ensembles of disclination quadrupoles given in Fig. 18.

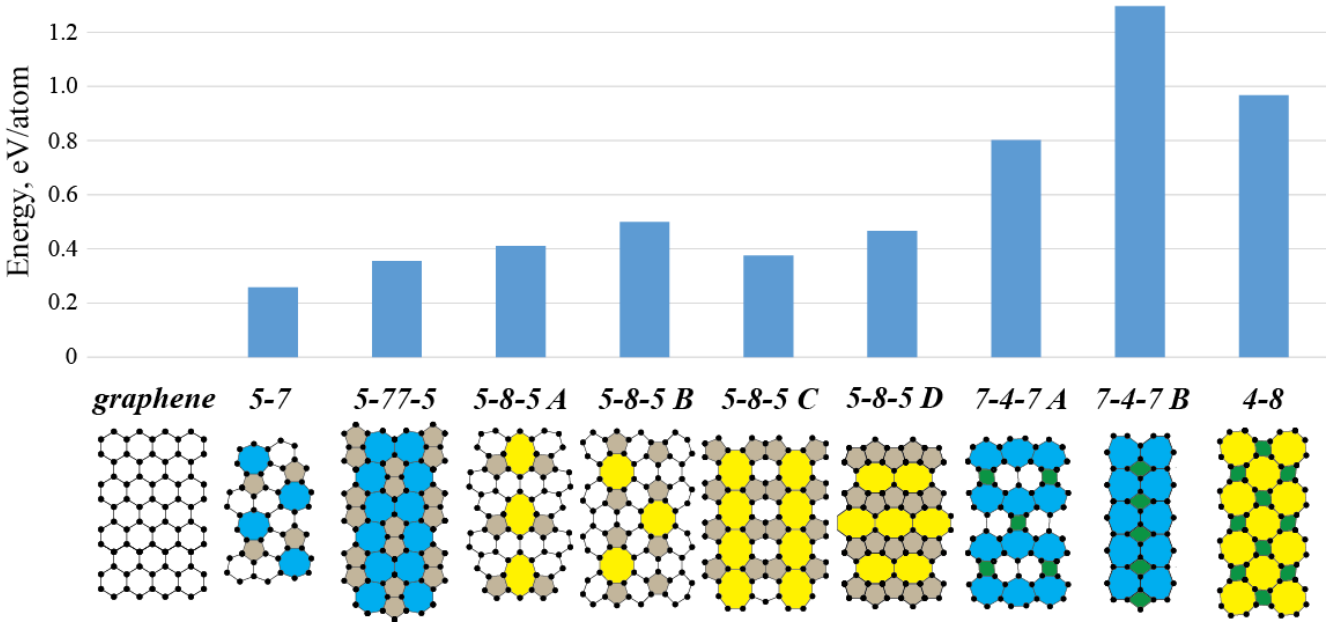

Fig. 20. Energy per carbon atom for pseudo-graphene crystals, given in Fig. 15.

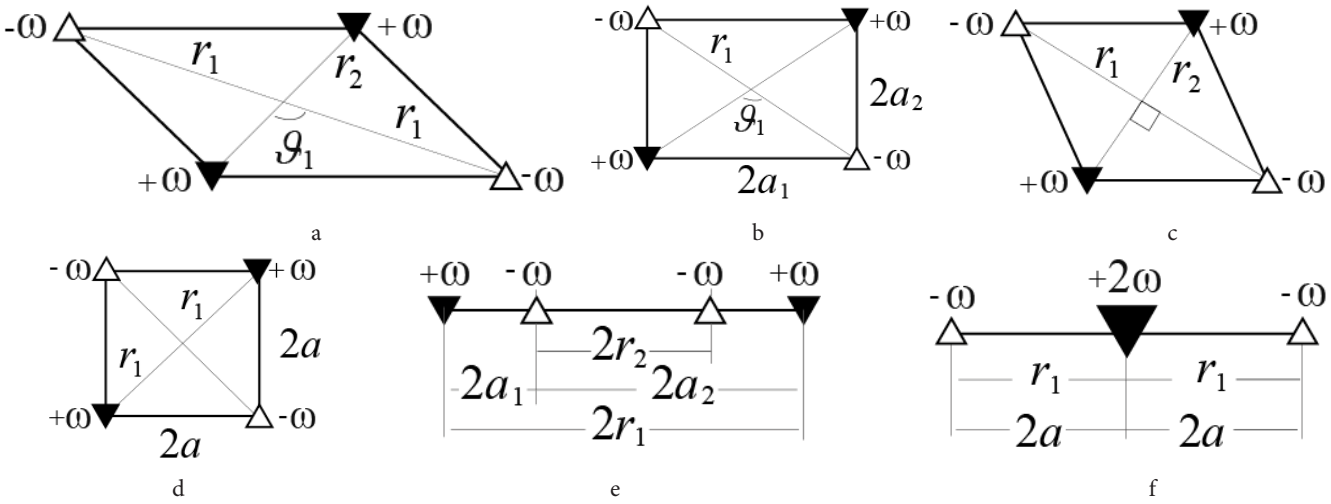

Fig. 21. Self-screened disclination quadrupoles. Parallelogram (a), special cases of parallelogram: a rectangle (b), a rhombus (c), a quadrate (d), and line quadrupoles (e, f) as degenerate parallelograms [43].

The energies of quadrupoles, shown in Fig. 21, have the following algebraic representations [64]:

(a) for the parallelogram (Fig. 21a)

$$E_{par}=\frac{G(1+\nu)\omega^2}{4\pi}\cdot \left(r_1^2\ln\frac{16r_1^4}{(r_1^2+r_2^2-2r_1r_2\cos\upsilon_1)(r_1^2+r_2^2+2r_1r_2\cos\upsilon_1)}+ r_2^2\ln\frac{16r_2^4}{(r_1^2+r_2^2-2r_1r_2\cos\upsilon_1)(r_1^2+r_2^2+2r_1r_2\cos\upsilon_1)}+ 2r_1r_2\cos\upsilon_1\ln\frac{r_1^2+r_2^2-2r_1r_2\cos\upsilon_1}{r_1^2+r_2^2+2r_1r_2\cos\upsilon_1}\right); \quad (11a)$$

(b) for the rectangle (Fig. 21b)

$$E_{rec}=\frac{G(1+\nu)\omega^2r_1^2}{2\pi}\cdot\left(\ln 4-(1-\cos\upsilon_1)\ln(1-\cos\upsilon_1)-(1+\cos\upsilon_1)\ln(1+\cos\upsilon_1)\right)= =\frac{G(1+\nu)\omega^2}{\pi}\left(a_1^2\ln\frac{a_1^2+a_2^2}{a_1^2}+a_2^2\ln\frac{a_1^2+a_2^2}{a_2^2}\right); \quad (11b)$$

(c) for the rhombus (Fig. 21c)

$$E_{rhomb}=\frac{G(1+\nu)\omega^2}{2\pi}\left(r_1^2\ln\frac{4r_1^2}{r_1^2+r_2^2}+r_2^2\ln\frac{4r_2^2}{r_1^2+r_2^2}\right); \quad (11c)$$

(d) for the square (Fig. 21d)

$$E_{qudr}=\frac{G(1+\nu)\omega^2r_1^2}{2\pi}\ln 2=\frac{2G(1+\nu)\omega^2a^2}{\pi}\ln 2; \quad (11d)$$

(e) for the line quadrupole (Fig. 21e)

$$E_{lq}=\frac{G(1+\nu)\omega^2}{2\pi}\cdot\left(r_1^2\ln\frac{4r_1^2}{r_1^2-r_2^2}+r_2^2\ln\frac{4r_2^2}{r_1^2-r_2^2}-2r_1r_2\ln\frac{r_1+r_2}{r_1-r_2}\right)=$$

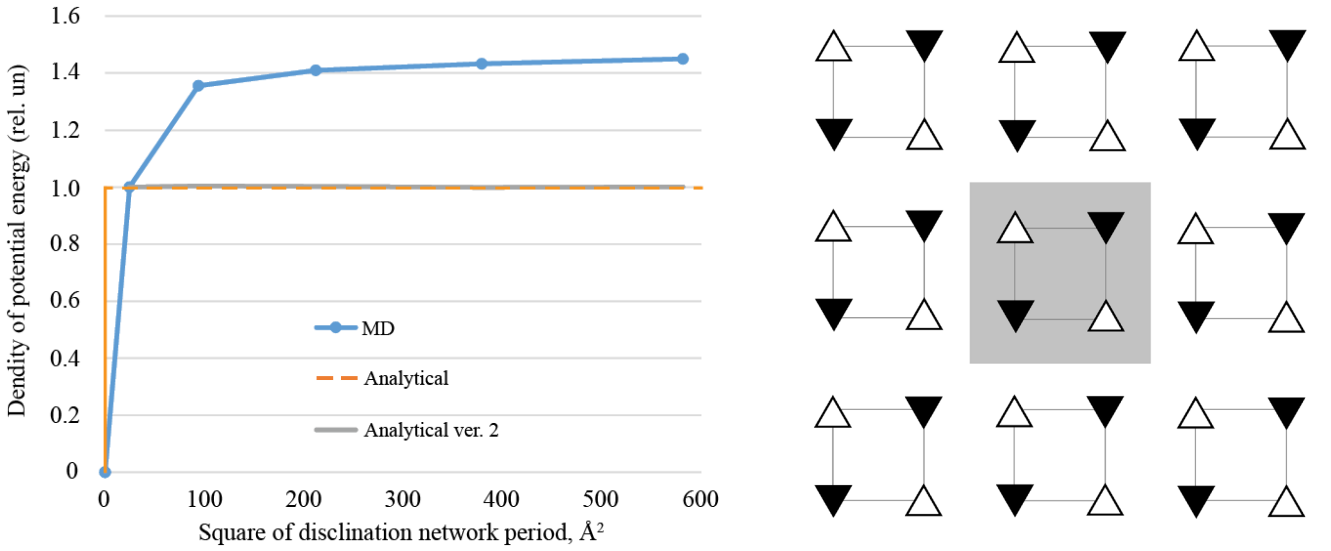

Fig. 22. Energy per unit area for pseudo-graphenes "4-8", as a function of the square of the DNDN period. The blue dots correspond to the energies calculated with the help of MD simulation; red and grey lines correspond to the dependences, calculated analytically taking into account 1 and 4 disclination quadrupoles, correspondingly. The energies are normalized to the energy of a tightly packed structure "4-8 g0" shown in Fig. 16a. In disclination scheme (right), the area related to the quadrupole used in analytical calculation of DN energy, is highlighted [64].

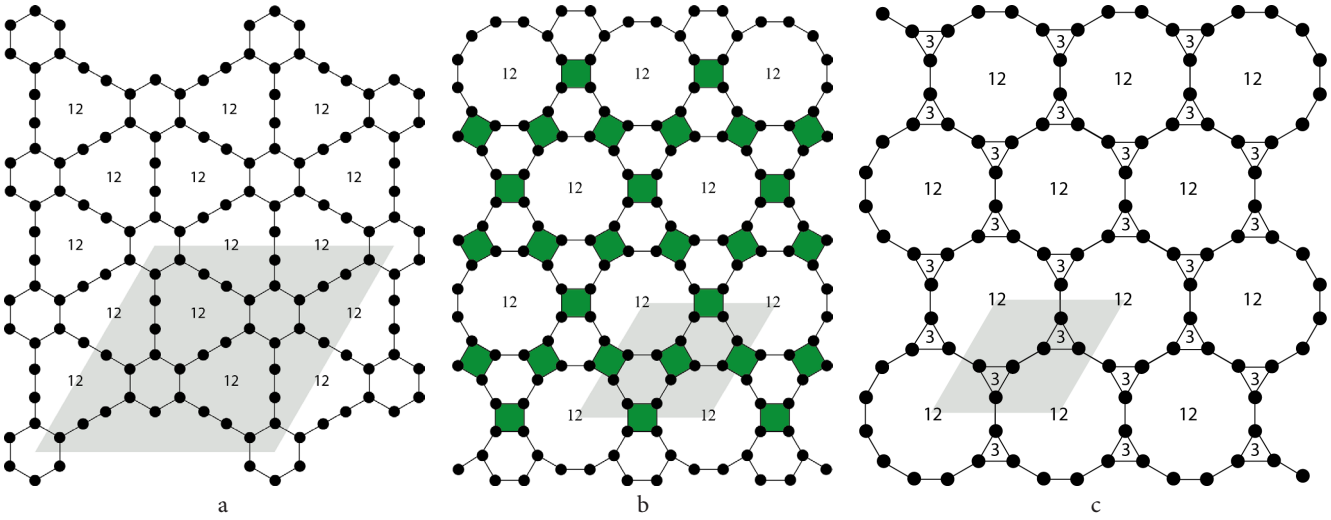

Fig. 23. Examples of exotic pseudo-graphene crystals (PGCs): graphyne (a) [66], 4-12 network (b) [67], 3-12 network (c) [68]. Shadowed areas in Figs. correspond to elementary cells of each pseudo-graphene, respectively.

$$= \frac{G(1+\nu)\omega^2}{\pi} \cdot \cdot \left(a_1^2 \ln \frac{a_2^2 - a_1^2}{a_1^2} + a_2^2 \ln \frac{a_2^2 - a_1^2}{a_2^2} + 2a_1 a_2 \ln \frac{a_2 + a_1}{a_2 - a_1} \right), \quad r_1 > r_2, \quad a_2 > a_1; \tag{11e}$$

(f) for the line quadrupole (Fig. 21f)

$$E_{lq} = \frac{G(1+\nu)\omega^2 r_1^2}{\pi} \ln 2 = \frac{4G(1+\nu)\omega^2 a^2}{\pi} \ln 2. \tag{11f}$$

For each crystal with a periodic DN, a suitable disclination quadrupole can be determined for calculating DN energy per unit area e_{DN}. For example, for phagraphene (Fig. 15a) this is the disclination quadrupole in the form of the parallelogram (Fig. 21a), for structure "5-7 B" (Fig. 15b) this is the rhombus (Fig. 21c), for structure "5-8-5 D" (Fig. 15d) this is the line quadrupole (Fig. 21f), and for structure "4-8" (Fig. 16a) this is the square (Fig. 21d).

In Fig. 22, the average energy per unit area for graphene-like structures from Fig. 16, is plotted as function of the square of the DN period. The energies are normalized to the energy of a tightly packed structure "4-8 g0". The dependences were found from MD simulations (Fig. 22, blue dots), calculated with Eq. (11d) (Fig. 22, red line), and calculated with Eq. (2) adopted to four quadrupoles (Fig. 22, grey line) [64]. In disclination scheme (right-hand part in Fig. 22), the area occupied by quadrupole when calculating the DN energy is highlighted.

The average energy of graphene-like structures with alternating disclination networks (DNs) remains practically unchanged with increasing DN period. The exceptions are the crystals with the densest DNs, *i.e.* PGs. Pseudo-graphenes are low-energy containing disclination defects configurations. The energies of PGs "5-7 A" and "5-7 B" exceed the energy of an ideal graphene by only 0.28 – 0.38 eV/atom.

4.4. More pseudo-graphenes

At present, none of the listed in this Section PGs have been experimentally observed. Still there is a lot of efforts to study theoretically the properties of such and other graphene-like crystals [66 – 68]. Examples of exotic PGs are shown in Fig. 23. The PG "5-7" (so-called phagraphene) has the smallest formation energy per carbon atom, and therefore it has the greatest chances to exist.

4.5. Properties of pseudo-graphenes

Mechanical properties. Influence of defects on mechanical properties of a graphene was not clarified experimentally until now, but there is a number of theoretical studies devoted to the matter [24, 69 – 73]. In all those publications, decreasing of mechanical properties with increase in defect density is predicted.

Though nucleation of defects in graphene lattice reduces Young modulus and strength, it is possible to observe interesting effects on other mechanical behavior. For example, in Ref. [69] the superplasticity of a graphene with the distributed defects was predicted. In Ref. [73] auxetic properties were described through the introduction of point defects in graphene lattice. The negative Poisson ratio was achieved for small deformations. The critical change in deformation behavior is shifted to higher deformations with increase in density of defects. In Ref. [72] the dependence between graphene Young modulus and thermal conductivity coefficient on vacancy or Stone-Wales (SW) defect concentration was found. Increasing of vacancy concentration led to decrease of Young modulus in the linear manner. For SW defects, there was a deviation from linear dependence and lower sensitivity of Young modulus to defect concentration.

Electronic properties. Pseudo-graphenes demonstrate semi-metal [65], metal [74] or semiconductor [75] electronic properties. The band gap can be opened to values greater than 3 eV, which can be attributed to wide-gap semiconductors [75].

Magnetic properties. Point defects can induce magnetism in graphene. Vacancies and impurity atoms make it possible to observe either ferromagnetic or antiferromagnetic behavior, depending on point defect combination [71]; a broken bond because of vacancy formation (Fig. 1b) induces the magnetic moment in graphene. In Ref. [76, 77] the dependence of magnetic moment of point defect concentration is presented.

5. Summary and conclusions

Graphene with 1D defects, *i.e.* interfaces and grain boundaries, demonstrates conducting or superconducting states along these defects that can be used in nanoelectronics and nanoengineering applications. Pseudo-graphene crystals with periodic distributions of point disclinations exhibit metallic, semi-metallic, or semiconducting types of conductivity with isotropic or anisotropic properties. By changing the type and density of defects, one can control the characteristics of graphene in a wide range. Although today none of pseudo-graphenes has been found experimentally, their stability is confirmed by theoretical calculations.

There is a number of important tasks for future analysis of graphene and graphene-like crystals with defects:

— detailed experimental studies of defects and their ensembles in 2D crystalline objects;

— elucidation of the effect of defects on the physical properties of graphene and development of the corresponding models;

— determination of the criteria and conditions for the nucleation of defects in graphene;

— understanding the role of graphene sheet edges and size of graphene islands on the properties.

We expect that the fabrication of disclinated graphenes will become possible by improving the methods of graphene crystal growth, precise control of the growth parameters and control of the substrate morphology. This together with theoretical background will open a new direction in graphene science and technology — graphene defect engineering.

Acknowledgments. MAR and ALK thank the Ministry of Education and Science of the Russian Federation for its support (Project No 3.3194.2017/4.6) and AER is grateful for the support the Russian Foundation for Basic Research (grant No 18-01-00884).

References

1. K.S. Novoselov, A.K. Geim, S. V Morozov, D. Jiang, Y. Zhang, S. V Dubonos, I. V Grigorieva, A.A. Firsov. Science. 306(5696), 666, (2004). DOI: 10.1126/science.1102896
2. K.F. Mak, C. Lee, J. Hone, J. Shan, T.F. Heinz. Phys. Rev. Lett. 105(13), 136805 (2010). DOI: 10.1103/PhysRevLett.105.136805
3. K.K. Kim, A. Hsu, X. Jia, S.M. Kim, Y. Shi, M. Hofmann, D. Nezich, J.F. Rodriguez-Nieva, M. Dresselhaus, T. Palacios. Nano Lett. 12(1), 161 (2012). DOI: 10.1021/nl203249a
4. H. Liu, A.T. Neal, Z. Zhu, Z. Luo, X. Xu, D. Tománek, P.D. Ye, ACS Nano. 8(4), 4033 (2014). DOI: 10.1021/nn501226z
5. K.S. Novoselov, A.K. Geim, S.V. Morozov, D. Jiang, M.I. Katsnelson, I.V. Grigorieva, S.V. Dubonos, A.A. Firsov. Nature. 438(7065), 197 (2005). DOI: 10.1038/nature04233
6. Y. Zhang, Y.-W. Tan, H.L. Stormer, P. Kim, Nature. 438(7065), 201 (2005). DOI: 10.1038/nature04235
7. K.S. Novoselov, Z. Jiang, Y. Zhang, S. V Morozov, H.L. Stormer, U. Zeitler, J.C. Maan, G.S. Boebinger, P. Kim, A.K. Geim, Science. 315(5817), 1379 (2007). DOI: 10.1126/science.1137201
8. F. Scarpa, S. Adhikari, A. Srikantha Phani. Nanotechnology. 20(6), 065709 (2009). DOI: 10.1088/0957-4484/20/6/065709
9. C. Lee, X. Wei, J.W. Kysar, J. Hone. Science. 321(5887), 385 (2008). DOI: 10.1126/science.1157996
10. P.R. Wallace. Phys. Rev. 71(9), 622 (1947).

DOI: 10.1103/PhysRev.71.622
11. A. H. Neto, F. Guinea, N. M. R. Peres, K. S. Novoselov, A. K. Geim. Rev. Mod. Phys. 81(1), 109 (2009). DOI: 10.1103/RevModPhys.81.109
12. T. Ando. NPG Asia Mater. 1(1), 17 (2009). DOI: 10.1038/asiamat.2009.1
13. A. Das, S. Pisana, B. Chakraborty, S. Piscanec, S. K. Saha, U. V. Waghmare, K. S. Novoselov, H. R. Krishnamurthy, A. K. Geim, A. C. Ferrari. Nat. Nanotechnol. 3(4), 210 (2008). DOI: 10.1038/nnano.2008.67
14. H. Yang, J. Heo, S. Park, H. J. Song, D. H. Seo, K.-E. Byun, P. Kim, I. Yoo, H.-J. Chung, K. Kim. Science. 336(6085), 1140 (2012). DOI: 10.1126/science.1220527
15. F. Bonaccorso, Z. Sun, T. Hasan, A. C. Ferrari. Nat. Photonics. 4(9), 611 (2010). DOI: 10.1038/nphoton.2010.186
16. S. J. Koester, Mo Li. IEEE J. Sel. Top. Quantum Electron. 20(1), 84 (2014). DOI: 10.1109/JSTQE.2013.2272316
17. C. R. Dean, A. F. Young, I. Meric, C. Lee, L. Wang, S. Sorgenfrei, K. Watanabe, T. Taniguchi, P. Kim, K. L. Shepard. Nat. Nanotechnol. 5(10), 722 (2010). DOI: 10.1038/nnano.2010.172
18. E. Kaxiras. Atomic and Electronic Structure of Solids. Cambridge, Cambridge University Press (2003).
19. L. Liu, M. Qing, Y. Wang, S. Chen. J. Mater. Sci. Technol. 31(6), 599 (2015). DOI: 10.1016/J.JMST.2014.11.019
20. H. Wang, Q. Wang, Y. Cheng, K. Li, Y. Yao, Q. Zhang, C. Dong, P. Wang, U. Schwingenschlögl, W. Yang. Nano Lett. 12(1), 141 (2012). DOI: 10.1021/nl2031629
21. R. R. Nair, I.-L. Tsai, M. Sepioni, O. Lehtinen, J. Keinonen, A. V. Krasheninnikov, A. H. Castro Neto, M. I. Katsnelson, A. K. Geim, I. V. Grigorieva. Nat. Commun. 4(1), 2010 (2013). DOI: 10.1038/ncomms3010
22. J. Kotakoski, A. V Krasheninnikov, U. Kaiser, J. C. Meyer, Phys. Rev. Lett. 106(10), 105505 (2011). DOI: 10.1103/PhysRevLett.106.105505
23. A. L. Kolesnikova, M. A. Rozhkov, I. Hussainova, T. S. Orlova, I. S. Yasnikov, L. V Zhigilei, A. E. Romanov. Rev. Adv. Mater. Sci. 52, 91 (2017).
24. R. Grantab, V. B. Shenoy, R. S. Ruoff. Science. 330(6006), 946 (2010). DOI: 10.1126/science.1196893
25. J. H. Warner, E. R. Margine, M. Mukai, A. W. Robertson, F. Giustino, A. I. Kirkland. Science 337(6091), 209 (2012). DOI: 10.1126/science.1217529
26. A. J. Stone, D. J. Wales. Chem. Phys. Lett. 128(5–6), 501 (1986). DOI: 10.1016/0009-2614(86)80661-3
27. K. Kim, Z. Lee, W. Regan, C. Kisielowski, M. F. Crommie, A. Zettl. ACS Nano. 5(3), 2142 (2011). DOI: 10.1021/nn1033423
28. J. Lahiri, Y. Lin, P. Bozkurt, I. I. Oleynik, M. Batzill. Nat. Nanotechnol. 5(5), 326 (2010). DOI: 10.1038/nnano.2010.53
29. O. V. Yazyev, S. G. Louie. Phys. Rev. B. 81(19), 195420 (2010). DOI: 10.1103/PhysRevB.81.195420
30. P. Koskinen, S. Malola, H. Häkkinen. Phys. Rev. B. 80(7), 073401 (2009). DOI: 10.1103/PhysRevB.80.073401
31. J. Gao, J. Yip, J. Zhao, B. I. Yakobson, F. Ding. J. Am. Chem. Soc. 133(13), 5009 (2011). DOI: 10.1021/ja110927p
32. J. Coraux, A. T. N'Diaye, M. Engler, C. Busse, D. Wall, N. Buckanie, F.-J. M. zu Heringdorf, R. van Gastel, B. Poelsema, T. Michely. New J. Phys. 11(2), 23006 (2009).
33. Z. H. Ni, H. M. Wang, Y. Ma, J. Kasim, Y. H. Wu, Z. X. Shen. ACS Nano. 2(5), 1033 (2008). DOI: 10.1021/nn800031m
34. Z. Cheng, Q. Zhou, C. Wang, Q. Li, C. Wang, Y. Fang. Nano Lett. 11(2), 767 (2011). DOI: 10.1021/nl103977d
35. C. J. Russo, J. A. Golovchenko. Proc. Natl. Acad. Sci. U. S. A. 109(16), 5953 (2012). DOI: 10.1073/pnas.1119827109
36. S. J. Stuart, A. B. Tutein, J. A. Harrison. J. Chem. Phys. 112(14), 6472 (2000). DOI: 10.1063/1.481208
37. J. Tersoff. Phys. Rev. Lett. 61(25), 2879 (1988). DOI: 10.1103/PhysRevLett.61.2879
38. https://openkim.org/dev-kim-item/LennardJones612_UniversalShifted__ MO_959249795837_002
39. P. Hohenberg, W. Kohn. Phys. Rev. 136(3B), B864 (1964). DOI: 10.1103/PhysRev.136.B864
40. J. P. Perdew, K. Burke, M. Ernzerhof. Phys. Rev. Lett. 77(18), 3865 (1996). DOI: 10.1103/PhysRevLett.77.3865
41. I. S. Yasnikov, A. L. Kolesnikova, A. E. Romanov. Phys. Solid State. 58(6), 1184 (2016). DOI: 10.1134/S1063783416060342
42. A. E. Romanov, V. I. Vladimirov. In: Dislocations in Solids (ed. by F. R. N. Nabarro). Amsterdam, North-Holland (1992) p. 191.
43. A. E. Romanov, A. L. Kolesnikova. Prog. Mater. Sci. 54(6), 740 (2009). DOI: 10.1016/j.pmatsci.2009.03.002
44. A. Richter, A. E. Romanov, W. Pompe, V. I. Vladimirov, Phys. Stat. Sol. B. 143(1), 43 (1987).
45. J. D. Eshelby. Proc. R. Soc. A. 241(1226), 376 (1957). DOI:10.1098/rspa.1957.0133
46. T. Mura. Micromechanics of Defects in Solids. Dordrecht/Boston/Lancaster, Martinus Nijhoff Publishers (1987).
47. A. L. Kolesnikova, T. S. Orlova, I. Hussainova, A. E. Romanov. Phys. Solid State. 56(12), 2573 (2014). DOI: 10.1134/S1063783414120166
48. A. L. Kolesnikova, M. Yu. Gutkin, A. E. Romanov. Rev. Adv. Mater. Sci. 51(2), 130 (2017).
49. F. Kroupa. In: Theory of Crystal Defects. Proceedings of the Summer School held in Hrazany in September 1964, Prague, Academia — Publishing House of the Czechoslovak Academy of Sciences (1966) p. 276.
50. A. L. Kolesnikova, R. M. Soroka, A. E. Romanov. Materials Physics and Mechanics. 17(1), 71 (2013).
51. R. De Wit. Continual Theory of Disclinations. Moscow, Mir (1977). (in Russian)
52. A. L. Kolesnikova, A. E. Romanov. Circular dislocation-disclination loops and their application to boundary problem solution in the theory of defects. Preprint No 1019, Leningrad, Phys.-Tech. Inst. (1986). (in Russian)
53. A. L. Kolesnikova, A. E. Romanov. Tech. Phys. Lett. 3(6), 272 (1987).
54. M. A. Rozhkov, A. L. Kolesnikova, T. S. Orlova, L. V. Zhigilei, A. E. Romanov. Mater. Phys. Mech. 29(1), 101 (2016).
55. A. E. Romanov, A. L. Kolesnikova, T. S. Orlova, I. Hussainova, V. E. Bougrov, R. Z. Valiev. Carbon. 81, 223 (2015). DOI: 10.1016/j.carbon.2014.09.053
56. J. Zhang, J. Zhao. Carbon. 55(1), 151 (2013). DOI: 10.1016/j.carbon.2012.12.021

57. V. V. Gertsman, A. A. Nazarov, A. E. Romanov, R. Z. Valiev, V. I. Vladimirov. Philos. Mag. A. 59(5), 1113 (1989). DOI: 10.1080/01418618908209841
58. A. A. Nazarov, A. E. Romanov, R. Z. Valiev. Acta Metal. Mater. 41(4), 1033 (1993). DOI: 10.1016/0956-7151(93)90152-I
59. Y. Liu, B. I. Yakobson. Nano Lett. 10(6), 2178 (2010). DOI: 10.1021/nl100988r
60. A. Bagri, S.-P. Kim, R. S. Ruoff, V. B. Shenoy. Nano Lett. 11(9), 3917 (2011). DOI: 10.1021/nl202118d
61. K. A. Ritter, J. W. Lyding. Nat. Mater. 8(3), 235 (2009). DOI: 10.1038/nmat2378
62. P. Koskinen, S. Malola, H. Häkkinen. Phys. Rev. Lett. 101(11), 115502 (2008). DOI: 10.1103/PhysRevLett.101.115502
63. M. Acik, Y. J. Chabal. Jpn. J. Appl. Phys. 50(7), 070101 (2011). DOI: 10.1143/jjap.50.070101
64. M. A. Rozhkov, A. L. Kolesnikova, I. S. Yasnikov, A. E. Romanov. Low Temp. Phys. 44(9), 918 (2018). DOI: 10.1063/1.5052677
65. Z. Wang, X.-F. Zhou, X. Zhang, Q. Zhu, H. Dong, M. Zhao, A. R. Oganov. Nano Lett. 15(9), 6182 (2015). DOI: 10.1021/acs.nanolett.5b02512
66. A. Mrozek, T. Burczyński. Comput. Assist. Methods Eng. Sci. 20(4), 309 (2017).
67. H. Zhu, A. T. Balaban, D. J. Klein, T. P. Živković. J. Chem. Phys. 101(6), 5281 (1994). DOI: 10.1063/1.467382
68. H. Sun, S. Mukherjee, M. Daly, A. Krishnan, M. H. Karigerasi, C. V. Singh. Carbon. 110, 443 (2016). DOI: 10.1016/j.carbon.2016.09.018
69. A. S. Kochnev, I. A. Ovid'ko, B. N. Semenov. Rev. Adv. Mater. Sci. 47, 79 (2016).
70. U. Sim, T.-Y. Yang, J. Moon, J. An, J. Hwang, J.-H. Seo, J. Lee, K. Y. Kim, J. Lee, S. Han. Energy Environ. Sci. 6(12), 3658 (2013). DOI: 10.1039/c3ee42106f
71. O. V. Yazyev, L. Helm. Phys. Rev. B. 75(12), 125408 (2007). DOI: 10.1103/PhysRevB.75.125408
72. F. Hao, D. Fang, Z. Xu. Appl. Phys. Lett. 99(4), 041901 (2011). DOI: 10.1063/1.3615290
73. J. N. Grima, S. Winczewski, L. Mizzi, M. C. Grech, R. Cauchi, R. Gatt, D. Attard, K. W. Wojciechowski, J. Rybicki. Adv. Mater. 27(8), 1455 (2015). DOI: 10.1002/adma.201404106
74. A. N. Enyashin, A. L. Ivanovskii. phys. status solidi. 248(8), 1879 (2011). DOI: 10.1002/pssb.201046583
75. A. N. Enyashin, A. L. Ivanovskii. Chem. Phys. Lett. 545, 78 (2012). DOI: 10.1016/j.cplett.2012.07.024
76. O. V. Yazyev. Phys. Rev. Lett. 101(3), 037203 (2008). DOI: 10.1103/PhysRevLett.101.037203
77. R. R. Nair, M. Sepioni, I.-L. Tsai, O. Lehtinen, J. Keinonen, A. V. Krasheninnikov, T. Thomson, A. K. Geim, I. V. Grigorieva. Nat. Phys. 8(3), 199 (2012). DOI: 10.1038/nphys2183